



HFF
18,7/8

Solution of thermo-fluid problems by collocation with local pressure correction

868

Gregor Kosec and Božidar Šarler

*Laboratory for Multiphase Processes, University of Nova Gorica,
Nova Gorica, Slovenia*

Received 15 May 2007
Revised 11 December 2007
Accepted 12 December 2007

Abstract

Purpose – The purpose of this paper is to explore the application of the mesh-free local radial basis function collocation method (RBF-CM) in solution of coupled heat transfer and fluid-flow problems.

Design/methodology/approach – The involved temperature, velocity and pressure fields are represented on overlapping five noded sub-domains through collocation by using multiquadrics radial basis functions (RBF). The involved first and second derivatives of the fields are calculated from the respective derivatives of the RBFs. The energy and momentum equations are solved through explicit time stepping.

Findings – The performance of the method is assessed on the classical two dimensional de Vahl Davis steady natural convection benchmark for Rayleigh numbers from 10^3 to 10^8 and Prandtl number 0.71. The results show good agreement with other methods at a given range.

Originality/value – The pressure-velocity coupling is calculated iteratively, with pressure correction, predicted from the local mass continuity equation violation. This formulation does not require solution of pressure Poisson or pressure correction Poisson equations and thus much simplifies the previous attempts in the field.

Keywords Flow, Convection, Pressure, Thermodynamics, Fluid dynamics

Paper type Research paper

1. Introduction

The most commonly used discrete approximate methods for solving systems of partial differential equations (PDEs) in fluid-flow problems are the finite difference method, the finite volume method, the finite element method, the spectral method and the boundary element method (BEM). Despite the suitability of the enumerated methods for solving fluid flow as well as other physical situations, there are still some substantial difficulties in applying them to realistic, geometrically complex three dimensional systems. The major problem is in creating a suitable mesh. The meshing (polygonisation) is often the most time consuming part of the solution process and is far from being fully automated. However, there is a rapidly emerging branch of numerical methods, where there is no need to create a polygonisation, neither in the domain nor on its boundary. The solution is represented on the arbitrarily distributed set of nodes without any additional topological relations between them. These meshfree methods represent a promising technique to avoid the meshing problems



(Atluri and Shen, 2002a, b; Atluri, 2004; Chen, 2002; Kansa, 1990a; Liu, 2003; Liu and Gu, 2005).

A number of mesh-reduction techniques such as the dual reciprocity BEM with radial basis functions (RBF) (Šarler and Kuhn, 1999), mesh-free techniques such as the dual reciprocity method with fundamental solutions (Šarler, 2002), meshfree local Petrov Galerkin methods (MLPG) (Atluri and Shen, 2002b, Lin and Atluri, 2001) have been developed for transport phenomena and solution of the Navier-Stokes equations. This paper is focused on the simplest class of mesh-free methods in development today, the radial basis function collocation methods (RBFCM) (Buhmann, 2000; Šarler, 2002, 2007).

The fluid-flow problem is a global problem in general. In order to solve such global problem, one needs to solve the global matrix (Šarler *et al.*, 2004; Šarler, 2005). Solving matrices for global systems with fine mesh or complex geometries can become a major numerical problem, therefore completely local scheme for solving fluid-flow problems is proposed in the present paper. This method represents a local variant of the already developed global RBFCM solution (Šarler, 2005), for coupled heat transfer and fluid flow problems. This local variant has been previously developed for diffusion problems (Šarler and Vertnik, 2006), convection-diffusion solid-liquid phase change problems (Vertnik and Šarler, 2006) and subsequently successfully applied in industrial process of direct chill casting (Vertnik *et al.*, 2006). The spectra of physics coped is extended to solution of coupled mass, energy and momentum equations in this paper. Instead of solving the pressure Poisson equation or/and pressure correction Poisson equation (Divo and Kassab, 2007), a much simplified local pressure-velocity coupling (LPVC) algorithm is proposed. The new algorithm is tested on classical de Vahl Davis (de Vahl Davis, 1983; Hortmann *et al.*, 1990; Manzari, 1999) natural convection problem. The results of the method are assessed in terms of streamfunction extreme, cavity Nusselt number, and mid-plane velocity components.

2. Governing equations

The steady-state natural convection problem is described by three coupled PDEs and Boussinesq approximation. The PDEs are mass, momentum and energy conservation equations where all material properties are considered to be constant. The equations are given as:

$$\nabla \cdot v = 0, \quad (1)$$

$$\nabla \cdot (\rho v v) = -\nabla P + \nabla \cdot (\mu \nabla v) + f, \quad (2)$$

$$\nabla \cdot (\rho c_p T v) = \nabla \cdot (\lambda \nabla T), \quad (3)$$

$$f = \rho [1 - \beta_B (T - T_{\text{ref}})] g, \quad (4)$$

with $v, P, T, \lambda, c_p, g, \rho, \beta_B, T_{\text{ref}}, \mu$ and f standing for velocity, pressure, temperature, thermal conductivity, specific heat, gravitational acceleration, density, coefficient of thermal expansion, reference temperature for Boussinesq approximation, viscosity and body force, respectively. The problem is solved on a fixed domain Ω with boundary Γ where Dirichlet and Neumann boundary conditions for temperature might be used and Dirichlet boundary conditions for velocity are used.

3. Solution procedure

In order to solve the problem, the time dependent variant of equations (2) and (3) is employed. The explicit time scheme is adopted to cope with the transience terms in momentum and energy equations. The Navier-Stokes equations (1) and (2) are solved iteratively. The LPVC algorithm, where pressure correction is estimated from local mass continuity violation, is used to drive the intermediate velocity towards the divergence-free velocity. The basic elements of the solution procedure are as follows:

In the first step, the velocity is estimated from the discretized transient form of equation (2):

$$\hat{v} = v_0 + \frac{\Delta t}{\rho} [-\nabla P_0 + \nabla \cdot (\mu \nabla v_0) + f_0 - \nabla \cdot (\rho v_0 v_0)], \quad (5)$$

where \hat{v} denotes velocity at time $t_0 + \Delta t$, v_0, P_0 denote velocity and pressure at time t_0 and Δt stands for the time-step length. The calculated velocity \hat{v} does not satisfy the mass continuity equation (1) in general. In order to couple mass continuity equation with the momentum equation, an iteration process is used where in the first iteration, the velocity and the pressure are set to:

$$\begin{aligned} v^m &= \hat{v}, \\ P^m &= P_0 \quad ; m = 1, \end{aligned} \quad (6)$$

where m stands for iteration index. To project the velocity into the divergence free space, a correction term \tilde{v} is added:

$$\nabla \cdot (v^m + \tilde{v}) = 0 \rightarrow \nabla \cdot v^m = -\nabla \cdot \tilde{v}. \quad (7)$$

The velocity correction is assumed to be affected only by effect of the pressure correction:

$$\tilde{v} = -\frac{\Delta t}{\rho} \nabla \tilde{P}, \quad (8)$$

where \tilde{P} stands for the pressure correction. The pressure correction Poisson equation is constructed by applying the divergence over equation (8):

$$\nabla^2 \tilde{P} = \frac{\rho}{\Delta t} \nabla \cdot v^m. \quad (9)$$

Instead of solving the equation (9) globally with the appropriate pressure correction boundary conditions (Divo and Kassab, 2007), the pressure correction is assumed to be linearly related to the Laplace of pressure correction. In the second step, the pressure correction is therefore calculated as:

$$\tilde{P} \approx L^2 \nabla^2 \tilde{P} = L^2 \frac{\rho}{\Delta t} \nabla \cdot v^m, \quad (10)$$

where L stands for characteristic length. The very important assumption (10) enables for solving the problem completely locally. In the third step, the intermediate pressure and velocity are corrected as:

$$P^{m+1} = P^m + \beta \tilde{P}, \quad v^{m+1} = v^m - \beta \frac{\Delta t}{\rho} \nabla \tilde{P}, \quad (11)$$

where β stands for suitable relaxation parameter. If the criteria:

$$\nabla \cdot v^{m+1} < \varepsilon_v, \quad (12)$$

is not met than the iteration returns back to the equation (10), else the pressure-velocity iteration is completed and the calculation proceeds to the next step.

The fourth step is to solve the transient form of the energy equation (3):

$$T = T_0 + \frac{\Delta t}{\rho c_p} [\nabla \cdot (\lambda \nabla T_0) - \nabla \cdot (\rho c_p T_0 v_0)], \quad (13)$$

where T_0 and T denote temperature at time t_0 and $t_0 + \Delta t$. The steady-state is achieved when the criteria:

$$\begin{aligned} \frac{|T - T_0|}{|T_0|} < \varepsilon_T; \quad T_0 \neq 0 \\ T < \varepsilon_T; \quad T_0 = 0 \end{aligned} \quad (14)$$

is met in all nodes. If the criteria (14) is not met, the body force is updated and calculation returns back to equation (5). The simulation flowchart is shown in Figure 1.

4. Radial basis function collocation method

The pressure, velocity and temperature fields are interpolated on the coincident grid points by Hardy's multiquadrics RBF. The arbitrary function θ is represented on each of the local sub-domains as:

$$\theta(\mathbf{p}) \approx \sum_{n=1}^N \alpha_n \Lambda_n(\mathbf{p}), \quad (15)$$

with \mathbf{p} , Λ_n , α_n and N standing for the position vector, the basis function, the collocation coefficient and the number of the collocation points, respectively. Hardy's multiquadrics basis functions are defined as:

$$\Lambda_n(\mathbf{p}) = \sqrt{r_n^2(\mathbf{p}) + c^2 r_0^2}; \quad r_n^2 = (\mathbf{p} - \mathbf{p}_n) \cdot (\mathbf{p} - \mathbf{p}_n), \quad (16)$$

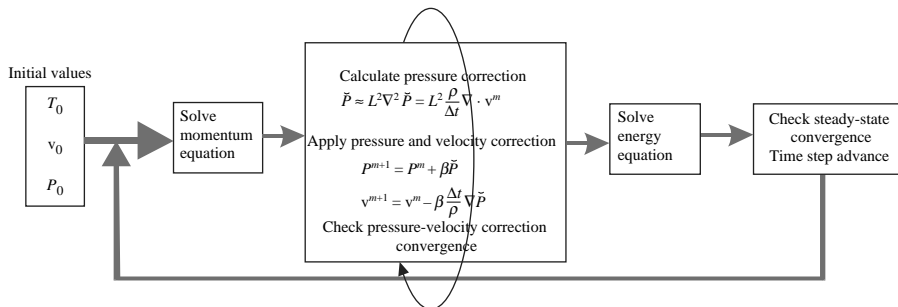


Figure 1. The calculation flowchart

where c represents a dimensionless shape parameter. The scaling parameter r_0^2 is set to the maximum nodal distance of the sub-domain. The coefficients α_n are obtained from the collocation condition which implies the exact satisfaction of the equation (15) in the nodal points where equation (15) must hold. In case, the number of the nodes is the same as the number of the terms in the series (15), the system simplifies to:

$$\theta(\mathbf{p}_i) = \theta_i = \sum_{n=1}^N \alpha_n \Lambda_n(\mathbf{p}_i), \quad (17)$$

$$\begin{bmatrix} \Lambda_{11} & \dots & \Lambda_{1N} \\ \dots & \dots & \dots \\ \Lambda_{N1} & \dots & \Lambda_{NN} \end{bmatrix} \begin{bmatrix} \alpha_1 \\ \dots \\ \alpha_N \end{bmatrix} = \begin{bmatrix} \theta_1 \\ \dots \\ \theta_N \end{bmatrix}, \quad (18)$$

where $\Lambda_{ni} = \Lambda_n(\mathbf{p}_i)$. Solution of the linear system of equation (18) provides the collocation coefficients α_n . Spatial derivatives of the function θ can be easily obtained through derivation of the equation (15):

$$\frac{\partial}{\partial p_\sigma} \theta(\mathbf{p}) \approx \sum_{n=1}^N \alpha_n \frac{\partial}{\partial p_\sigma} \Lambda_n(\mathbf{p}), \quad (19)$$

$$\frac{\partial^2}{\partial^2 p_\sigma} \theta(\mathbf{p}) \approx \sum_{n=1}^N \alpha_n \frac{\partial^2}{\partial^2 p_\sigma} \Lambda_n(\mathbf{p}), \quad (20)$$

where $p_{\sigma=x,y}$ stands for Cartesian coordinates. All necessary derivatives to construct the involved divergence, gradient and Laplace operators can be calculated through equations (19) and (20). The integral of function θ over p_σ (used in the present context in calculation of the stream function) can be evaluated as well:

$$\int \theta(\mathbf{p}) dp_\sigma = \sum_{n=1}^N \alpha_n \int \Lambda_n(\mathbf{p}) dp_\sigma. \quad (21)$$

All matrix elements Λ_{ni} and coefficients α_n need to be evaluated only once before time stepping begins.

Only the simplest sub-domain of five points is used within the overlapping collocation sub-domain strategy of the present paper. The described collocation method and sub-domain selection is schematically shown in Figure 2, where a five noded collocation sub-domain is used to approximate the first and the second spatial derivatives in the central node. The derivative instead of the function value is prescribed at the boundary collocation points with the Neumann boundary conditions. The equation (17) is replaced with:

$$\frac{\partial}{\partial p_\sigma} \theta(\mathbf{p}_i) = \sum_{n=1}^N \alpha_n \frac{\partial}{\partial p_\sigma} \Lambda_n(\mathbf{p}_i), \quad (22)$$

in such points. The index i stands for node where derivative is known.

5. Numerical examples

The classical de Vahl Davis (1983) natural convection problem is considered for benchmarking purposes. The domain of the problem (Figure 3) is a closed air filled (Prandtl number = 0.71) square cavity with differentially heated vertical walls ($\Delta T = T_H - T_C$) and insulated horizontal walls.

The steady-state is achieved through a time transient from the initial temperature, pressure and velocity all set to zero. All results are stated in Cartesian coordinates and standard dimensionless form (Wan *et al.*, 2001):

$$x = \frac{\bar{x}}{L}, \quad y = \frac{\bar{y}}{L}, \quad u = \frac{\bar{u}L\rho c_p}{\lambda}, \quad v = \frac{\bar{v}L\rho c_p}{\lambda}, \quad \Psi = \frac{T - T_C}{T_H - T_C}, \quad (23)$$

$$\Gamma = t \frac{\lambda}{\rho c_p L^2},$$

where x, y stand for the dimensionless coordinates, u, v stand for the dimensionless horizontal and vertical velocity components, Ψ stands for the dimensionless temperature and τ stands for the dimensionless time. Prandtl and Rayleigh numbers are calculated from the expressions:

$$Pr = \frac{\mu c_p}{\lambda}, \quad (24)$$

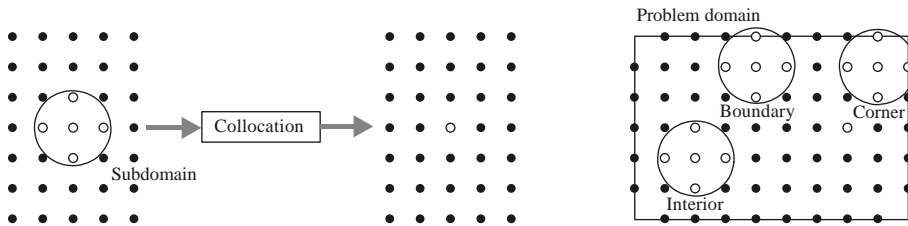


Figure 2. Local collocation scheme (left) and collocation sub-domain selection strategy (right)

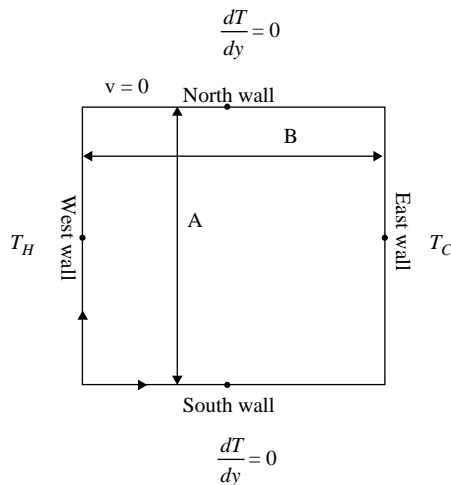


Figure 3. The problem description

$$Ra = \frac{g\beta\Delta TL^3\rho^2c_p}{\lambda\mu}, \quad (25)$$

where ΔT stands for maximum temperature difference and L stands for enclosure length.

Non-permeable and no slip (due to consideration of viscid fluid) boundary conditions are adopted on the whole boundary Γ :

$$v_\Gamma = 0. \quad (26)$$

The results are presented in terms of stream functions and temperature contours in Figure 4 and mid-plane velocities in Figure 5, respectively. The temperature contour plot step is 0.05 for all cases while streamfunction contour plot step is 0.1 for $Ra = 10^3$, 0.5 for $Ra = 10^4$, 1 for $Ra = 10^5$ and $Ra = 10^6$ and 5 for $Ra = 10^7$ and $Ra = 10^8$. In order to enable a straightforward numerical comparison, the mid-plane velocity values are stated in Table I, as well.

A comparison of our results (Table II) with the other similar attempts is done for the maximum mid-plane velocities, the mid-point stream function value, and the average Nusselt number on hot or cold wall where the results of the present study are compared with de Vahl Davis (1983), Sadat and Couturier (2000), Wan *et al.* (2001) and Šarler (2005) the streamfunction ψ is calculated through integration of the velocity component:

$$\psi(x, y) = \int u(x, y)dy. \quad (27)$$

The Nusselt number is calculated locally on the support of five collocation nodes through expression:

$$Nu(x, y) = -\frac{\partial\Psi(x, y)}{\partial x} + u(x, y)\Psi(x, y). \quad (28)$$

Our simulations are performed on 41×41 (with $N_{\max} = 1,677$), 81×81 (with $N_{\max} = 6,557$) and 101×101 (with $N_{\max} = 10,197$) grid sizes, where N_{\max} stands for the total number of the grid points. Additional check on the global mass conservation of the method is done by considering the time dependent mass continuity equation (1) globally, to check the numerical mass leakage. The following equation is implemented:

$$\bar{\rho}(t + \Delta t) = \bar{\rho}(t) - \Delta t\rho_0 \frac{1}{N_{\max}} \sum_{n=1}^{N_{\max}} \nabla \cdot v_n; \quad \bar{\rho}(t = 0) = \rho_0, \quad (29)$$

where $\bar{\rho}(t)$ stands for time dependent global density. The global density change is introduced as:

$$\Delta\rho = |\rho_0 - \bar{\rho}(N_t\Delta t)|, \quad (30)$$

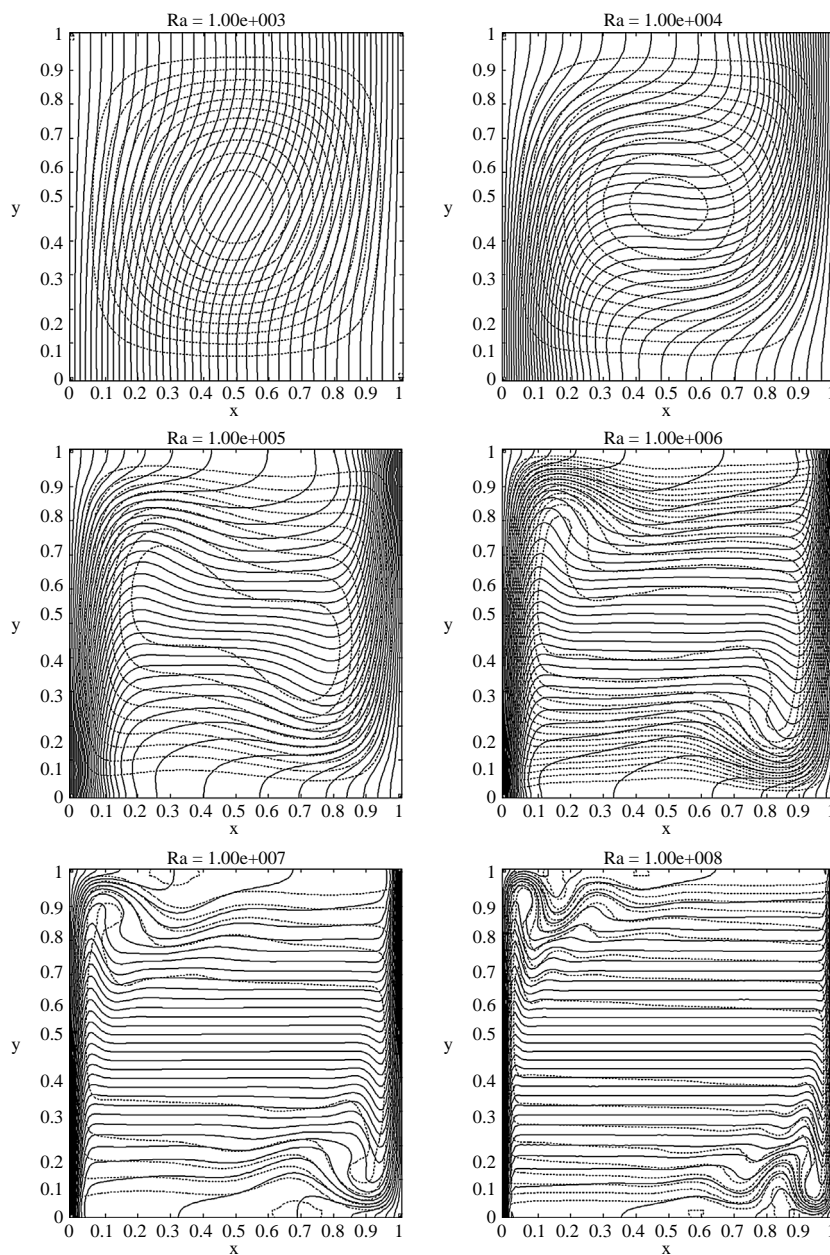


Figure 4.
Temperature contours (solid line) and streamline plots (dotted line)

where N_t stands for the number of time-steps. The relative density changes $\Delta\rho/\rho_0$ occurring as a function of different Rayleigh numbers for calculation with the grid density 101×101 are stated in Table III. The time-step criteria $\epsilon_T < 10^{-5}$ is used in all cases while pressure-velocity iteration criteria varies for different Rayleigh number

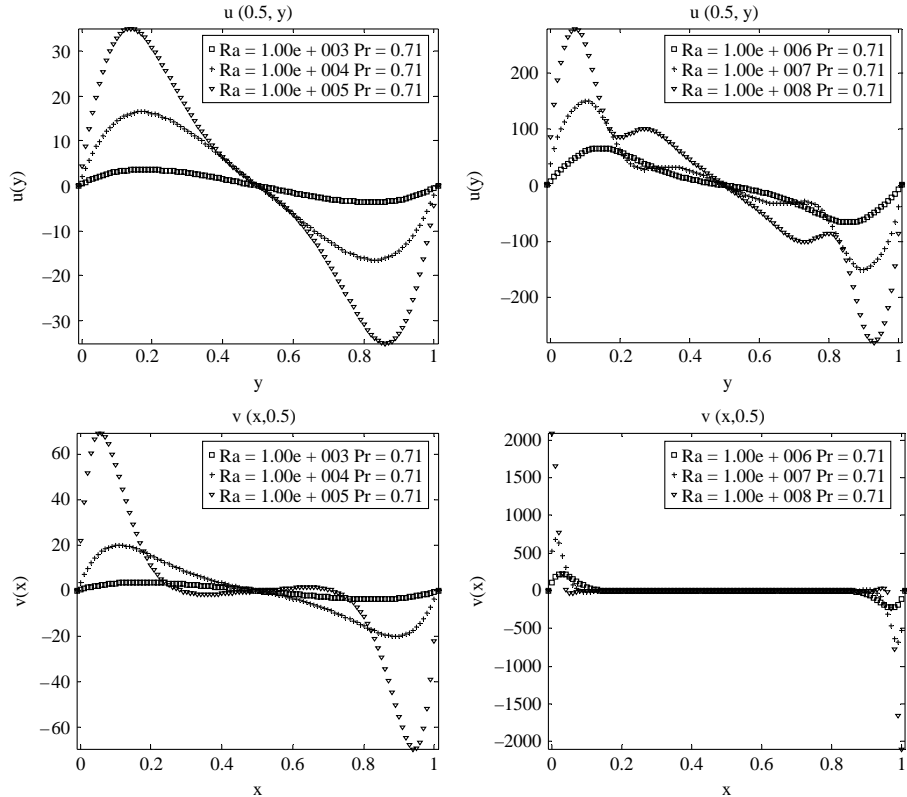


Figure 5.
Mid-plane velocities

(Table III). The time-step varies for different Rayleigh numbers, as well. The time-steps were determined by seeking the convergent scenario. The relaxation parameter is set to same value as dimensionless time-step in all cases. The number of pressure-velocity iterations, time-steps and actual calculation time for different Rayleigh numbers and grid sizes are stated in Table III, as well. All cases are calculated with RBF shape parameter $c = 30$. This issue is justified by the sensitivity study, given in the Appendix.

5.1 Numerical implementation and discussion of the results

Numerical implementation is done in C++ programming language in double precision and compiled with Intel C++ 9.1 compiler. The LAPACK routines are used to solve the LU decomposition. The parallelisation is implemented with OpenMP library with maximum $1.85 \times$ speedup factor achieved for two CPU cores. All calculations are done on a laptop computer Toshiba Satellite 100, with duo core Intel 2.16 GHz processor and 1 Gb of RAM. Approximately, 1, 5 and 8 Mb of RAM storage are required for grid densities 41×41 , 81×81 and 101×101 . The pressure correction requires only one step and therefore the algorithm needs small number of calculations per iteration cycle and this makes the algorithm fast and robust. Each pressure-velocity coupling iteration

x/y	0.000	0.05	0.1	0.15	0.2	0.25	0.3	0.35	0.4	0.45	0.5	Ra
u	0.000	1.922	3.042	3.572	3.655	3.421	2.958	2.337	1.611	0.820	0.000	10^3
v	0.000	2.044	3.182	3.669	3.681	3.377	2.865	2.226	1.515	0.765	0.000	10^4
u	0.000	8.884	14.084	16.358	16.406	14.961	12.575	9.665	6.511	3.264	0.000	10^5
v	0.000	14.680	19.929	19.411	16.113	12.195	8.647	5.768	3.503	1.646	0.000	10^5
u	0.000	20.218	32.133	35.340	31.839	25.018	17.704	11.462	6.690	3.048	0.000	10^5
v	0.000	67.778	60.088	33.245	13.201	3.262	-0.529	-1.453	-1.222	-0.672	0.000	10^6
u	0.000	34.504	58.012	66.594	60.433	46.729	32.256	20.208	11.356	5.009	0.000	10^6
v	0.000	209.729	65.587	1.637	-5.770	-1.393	0.753	0.789	0.545	0.171	0.000	10^7
u	0.000	115.470	149.670	129.797	69.256	32.989	30.303	33.201	27.256	14.515	0.000	10^7
v	0.000	294.796	-14.001	-0.395	0.004	0.176	0.357	0.109	0.423	0.006	0.000	10^8
u	0.000	248.453	266.354	149.301	86.413	96.987	97.311	74.817	47.606	23.062	0.000	10^8
v	0.000	7.726	-0.973	1.560	-0.418	0.392	0.154	-0.015	0.186	-0.041	0.000	10^8

Table I.
Values of mid-plane
velocity components
 u and v

Ra	v_{\max}	y	u_{\max}	x	\overline{Nu}	ψ_{mid}	References/discretization
10^3	3.679	0.179	3.634	0.813	1.116	1.174	de Vahl Davis (1983)
	3.686	0.188	3.489	0.813	1.117		Wan <i>et al.</i> (2001)
	3.566		3.544			1.165	Šarler (2005)
	3.991	0.170	3.931	0.825	1.101	1.298	41×41
	3.699	0.177	3.653	0.812	1.098	1.194	81×81
10^4	3.695	0.179	3.645	0.820	1.089	1.196	101×101
	19.51	0.120	16.24	0.823	2.234	5.098	de Vahl Davis (1983)
	19.79	0.120	16.17	0.823	2.243		Wan <i>et al.</i> (2001)
	19.04		15.80			4.971	Šarler (2005)
	19.81	0.120	16.24	0.825	2.075	5.155	41×41
10^5	19.83	0.120	16.27	0.825	2.120	5.167	81×81
	20.03	0.120	16.45	0.830	2.258	5.240	101×101
	68.22	0.066	34.81	0.855	4.510	9.142	de Vahl Davis (1983)
	68.52	0.064	34.63	0.852	4.534	9.092	Sadat and Couturier (2000)
	70.63	0.072	33.39	0.835	4.520		Wan <i>et al.</i> (2001)
106	67.59		32.51			8.907	Šarler (2005)
	67.65	0.070	33.67	0.850	4.624	8.896	41×41
	68.98	0.062	34.60	0.850	4.813	9.135	81×81
	69.69	0.069	35.03	0.860	4.511	9.278	101×101
	216.75	0.038	65.33	0.851	8.798	16.53	de Vahl Davis (1983)
107	219.41	0.038	64.43	0.852	8.832	16.29	Sadat and Couturier (2000)
	227.11	0.04	65.4	0.86	8.8		Wan <i>et al.</i> (2001)
	211.67		61.55			15.91	Šarler (2005)
	195.98	0.045	63.73	0.850	6.1	15.15	41×41
	219.48	0.038	64.87	0.851	7.67	16.13	81×81
108	221.37	0.039	65.91	0.860	8.97	16.51	101×101
	687.43	0.023	145.68	0.888	16.59	28.23	Sadat and Couturier (2000)
	714.48	0.022	143.56	0.922	16.65		Wan <i>et al.</i> (2001)
	632.60	0.020	127.70	0.925	10.43	24.93	41×41
	654.803	0.035	143.55	0.902	14.70	27.51	81×81
108	687.20	0.021	149.61	0.900	16.92	28.61	101×101
	2180.1	0.011	319.19	0.943	30.94	50.81	Sadat and Couturier (2000)
	2259.08	0.012	296.71	0.93	31.48		Wan <i>et al.</i> (2001)
	2060.86	0.010	264.96	0.939	29.33	44.85	81×81
	2095.23	0.009	278.49	0.930	32.12	47.12	101×101

Table II.
Comparison of the present method with previously published results

takes the same order of CPU time (t_{Pvi}) as the adjacent time step calculation. The time spent for pressure correction can be estimated from $t_{\text{Pvi}} = t_c N_{\text{Pvi}} / (N_{\text{Pvi}} + N_t)$. Good agreement with other methods at a given range (Rayleigh number from 10^3 to 10^8 and grid density with maximum 101×101 grid points) is achieved with the proposed algorithm. Our method over-predicts reference results for low-Rayleigh numbers but for higher Rayleigh numbers it under-predicts reference results. For Rayleigh number $Ra = 10^3$ current method over-predicts all reference results. Similar behaviour is observed for results with $Ra = 10^4$, but for $Ra = 10^5$ and $Ra = 10^6$ our method over-predicts only two of the three reference results. Finally, for $Ra = 10^7$ and $Ra = 10^8$ current method under-predicts both comparison results. High deviance from results (Wan *et al.*, 2001) at a high Rayleigh number is due to grid selection. The present results are calculated on an entirely uniform grid. The results (Wan *et al.*, 2001) are calculated on Gauss-Lobatto grid, which is a more suitable selection due to the

Ra	ϵ_v	41×41			81×81			101×101				
		$\Delta\tau$	N_t	$t_c[s]$	$\Delta\tau$	N_t	$t_c[s]$	$\Delta\tau$	N_t	$t_c[s]$		
10^3	$10e^{-4}$	$1e^{-04}$	3,208	22,750	$1e^{-04}$	190	26,837	$5e^{-05}$	22,750	525	3662	$3.37e^{-007}$
10^4	$10e^{-3}$	$1e^{-04}$	3,154	16,940	$1e^{-04}$	92	3,259	$5e^{-05}$	16,940	398	3706	$8.44e^{-006}$
10^5	$10e^{-2}$	$1e^{-04}$	1,590	13,690	$1e^{-04}$	70	1,244	$5e^{-05}$	13,690	329	4090	$1.06e^{-005}$
10^6	1	$1e^{-04}$	5,527	10,200	$1e^{-04}$	66	5,608	$1e^{-05}$	10,200	1486	55043	$1.38e^{-004}$
10^7	5	$1e^{-05}$	18,250	12,500	$1e^{-05}$	513	71,340	$5e^{-06}$	62,500	2597	184697	$3.01e^{-004}$
10^8	25				$5e^{-06}$	1,225	193,708	$5e^{-06}$	135,000	2938	219885	$5.90e^{-004}$

Table III.
Pressure-velocity
iteration criteria ϵ_v ,
time-step $\Delta\tau$, number of
pressure-velocity
correction iterations N_{Pvi} ,
number of time-steps
 t_{max} , actual CPU time
consumption t_c and
global density loss $\Delta\rho/\rho$

highest velocities in the boundary layer (Figure 5). The effect is more intense with the higher Rayleigh numbers and so the deviance between the results grows with the higher Rayleigh numbers.

6. Conclusions

This paper explores the local RBFCM approach in solution of the coupled heat transfer and fluid flow problems by using the simplified entirely local pressure correction. The algorithm is very simple to implement numerically, fast and robust. The algorithm can be efficiently and straightforwardly parallelized because of its local subdomain nature and explicit time stepping. This two important features enables the exploiting of the full power of the multi core platforms. A remark should be made in the sense that there are possible difficulties when working with finer grids than in present paper. The proposed algorithm includes only few surrounding points to calculate pressure correction. The present pressure correction calculation (calculated only from closest neighbouring points) may not be efficient enough when working with finer grids (200×200 or finer) and high-Rayleigh numbers (more than 5×10^7). Possible upgrade is to include wider domain of points in the pressure correction calculation. These topics are subject of further investigations, as well as focus on more complex geometries and more complex physical models (porous media, solidification, . . .), which seem to be quite simple to numerically implement in the present context. The investigation on the adaptive time dependent grid to enhance the accuracy and to avoid the eventual stability problems, the implementation of the characteristic-based-split algorithm (Massarotti *et al.*, 1998), the implementation of different sub-domain strategies, etc. all represents open issues, connected with the present method.

References

- Atluri, S.N. (2004), *The Meshless Method (MLPG) for Domain and BIE Discretization*, Tech Science Press, Encino, CA.
- Atluri, S.N. and Shen, S. (2002a), *The Meshless Method*, Tech Science Press, Encino, CA.
- Atluri, S.N. and Shen, S. (2002b), "The meshless local Petrov-Galerkin (MLPG) method: a simple & less-costly alternative to the finite element and boundary element methods", *Computer Modelling in Engineering & Sciences*, Vol. 3, pp. 11-52.
- Buhmann, M.D. (2000), *Radial Basis Functions*, Cambridge University Press, Cambridge.
- Chen, W. (2002), "New RBF collocation schemes and kernel RBFs with applications", *Lecture Notes in Computational Science and Engineering*, Vol. 26, pp. 75-86.
- de Vahl Davis, G. (1983), "Natural convection of air in a square cavity: a bench mark numerical solution", *International Journal of Numerical Methods in Fluids*, Vol. 3, pp. 249-64.
- Divo, E. and Kassab, A.J. (2007), "An efficient localized RBF meshless method for fluid flow and conjugate heat transfer", *ASME Journal of Heat Transfer*, Vol. 129, pp. 124-36.
- Hortmann, M., Perić, M. and Scheuerer, G. (1990), "Finite volume multigrid prediction of laminar natural convection – bench-mark solutions", *International Journal for Numerical Methods in Fluids*, Vol. 11, pp. 189-207.
- Kansa, E.J. (1990a), "Multiquadrics – a scattered data approximation scheme with application to computational fluid dynamics, Part I", *Computers and Mathematics with Applications*, Vol. 19, pp. 127-45.

-
- Lin, H. and Atluri, S.N. (2001), "Meshless local Petrov Galerkin method (MLPG) for convection-diffusion problems", *Computer Modelling in Engineering & Sciences*, Vol. 1, pp. 45-60.
- Liu, G.R. (2003), *Mesh Free Methods*, CRC Press, Boca Raton, FL.
- Liu, G.R. and Gu, Y.T. (2005), *An Introduction to Meshfree Methods and Their Programming*, Springer, Dordrecht.
- Manzari, M.T. (1999), "An explicit finite element algorithm for convection heat transfer problems", *International Journal of Numerical Methods for Heat and Fluid Flow*, Vol. 9, pp. 860-77.
- Massarotti, N., Nithiarasu, P. and Zienkiewicz, O.C. (1998), "Characteristic-based-split (CBS) algorithm for incompressible flow problems with heat transfer", *International Journal of Numerical Methods for Heat and Fluid Flow*, Vol. 8, p. 969.
- Sadat, H. and Couturier, S. (2000), "Performance and accuracy of a meshless method for laminar natural convection", *Numerical Heat Transfer, Part B*, Vol. 37.
- Šarler, B. (2002), "Towards a mesh-free computation of transport phenomena", *Engineering Analysis with Boundary Elements*, Vol. 26, pp. 731-8.
- Šarler, B. (2005), "A radial basis function collocation approach in computational fluid dynamics", *Computer Modelling in Engineering & Sciences*, Vol. 7, pp. 185-93.
- Šarler, B. (2007), *From Global to Local Radial Basis Function Collocation Method for Transport Phenomena*, Springer, Berlin, pp. 257-82.
- Šarler, B. and Kuhn, G. (1999), "Primitive variable dual reciprocity boundary element method solution of incompressible Navier-Stokes equations", *Engineering Analysis with Boundary Elements*, Vol. 23, pp. 443-55.
- Šarler, B. and Vertnik, R. (2006), "Meshfree explicit local radial basis function collocation method for diffusion problems", *Computers and Mathematics with Applications*, Vol. 51, pp. 1269-82.
- Šarler, B., Perko, J. and Chen, C.S. (2004), "Radial basis function collocation method solution of natural convection in porous media", *International Journal of Numerical Methods for Heat & Fluid Flow*, Vol. 14, pp. 187-212.
- Vertnik, R. and Šarler, B. (2006), "Meshless local radial basis function collocation method for convective-diffusive solid-liquid phase change problems", *International Journal of Numerical Methods for Heat and Fluid Flow*, Vol. 16, pp. 617-40.
- Vertnik, R., Založnik, M. and Šarler, B. (2006), "Solution of transient direct-chill aluminium billet casting problem with simultaneous material and interphase moving boundaries by a meshless method", *Engineering Analysis with Boundary Elements*, Vol. 30, pp. 847-55.
- Wan, D.C., Patnaik, B.S.V. and Wei, G.W. (2001), "A new benchmark quality solution for the buoyancy-driven cavity by discrete singular convolution", *Numerical Heat Transfer, Part B*, Vol. 40, pp. 199-228.

Appendix. The influence of the dimensionless shape parameter on the results

The convergence of the present RBF method was systematically studied in previous works for diffusive and convective diffusive problems (Šarler and Vertnik, 2006; Vertnik and Šarler, 2006), where it has been shown that the method converges.

The dimensionless shape parameter is set to 30 in all calculations in the preset paper. In order to justify this selection, a preliminary analysis has been done, described in this Appendix. For grid density 81×81 , all cases have been recalculated with different selection of the shape parameter. In order to measure the influence of the shape parameter on the results, the following deviation has been introduced:

$$D = \frac{\max|v|}{\max|v_{120}|} \tag{A.1}$$

where max stands for maximum and v_{120} stands for velocity calculated with $c = 120$. From Figure A1, it is evident that $c = 30$ represents a reasonable choice for the shape parameter in all cases. The results are not sensitive to increase of the value of the shape parameter over 30, however, setting high-shape parameter produces ill-conditioned matrix in equation (18). The choice of shape parameter represents a compromise between accuracy and ill-condition of the matrices, respectively. This behaviour has been observed also in our previous works (Šarler and Vertnik, 2006; Vertnik and Šarler, 2006).

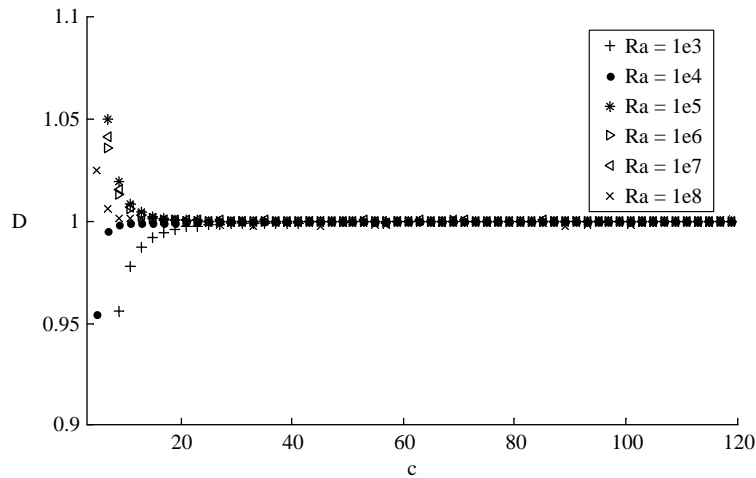


Figure A1.
Deviation of the final result with respect to the shape parameter

Corresponding author
Božidar Šarler can be contacted at: bozidar.sarler@p-ng.si